Tin-Based Composite Oxide Confined by Reduced Graphene Oxide as a High-Rate Anode for Sodium-Ion Capacitors

Yongmei Sun[a,b], Qingwen Fan[a], Chaoyun Song[c], Hailin Cong[d], Sanwei Hao[d], Mei Ma [b]*, and Peng Fu [a]*

[a]College of Agricultural Engineering and Food Science, Shandong University of Technology, Zibo 255000, P. R. China.

[b]School of Chemistry and Chemical Engineering, Shandong University of Technology, Zibo 255000, P. R. China.

[c]Department of Engineering, Strand Campus, King's College London, London, WC2R 2LS, United Kingdom.

[d]School of Materials Science and Engineering, Shandong University of Technology, Zibo 255000, Shandong, China

*Corresponding Authors.

Email addresses: mamei@sdut.edu.cn, fupengsdut@163.com

Table S1. Comparison of XRD Peak FWHM and Crystallite Size between $Sn_2P_2O_7$ and $Sn_2P_2O_7$/rGO

Peak Position (2θ)	FWHM (°) $Sn_2P_2O_7$	FWHM (°) $Sn_2P_2O_7$/rGO	Crystallite Size (nm) $Sn_2P_2O_7$	Crystallite Size (nm) $Sn_2P_2O_7$/rGO
20.2666	0.0513	0.0107	155.6697	
20.4805	0.0182	0.5395		14.7986
21.3751	0.0129	0.0156		
21.6668	0.0113	0.2683		29.8116
31.2935	0.2282	0.3082		
36.0582	0.2622	0.0194	31.5136	
36.0971	0.0160	0.3171		

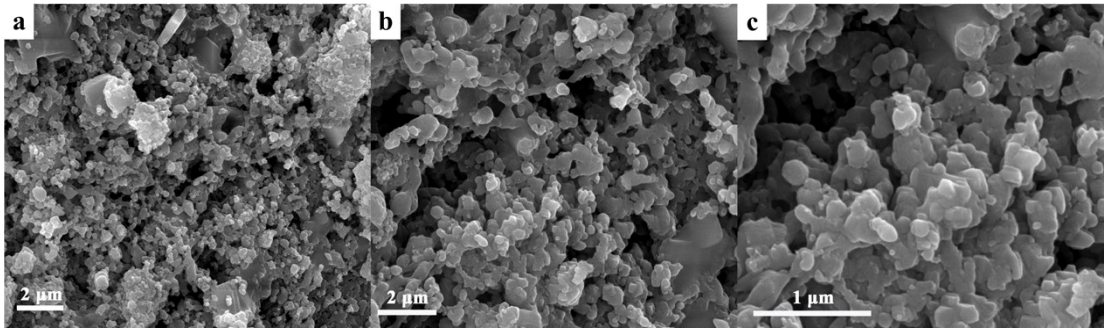

Figure S1. SEM images of $Sn_2P_2O_7$.

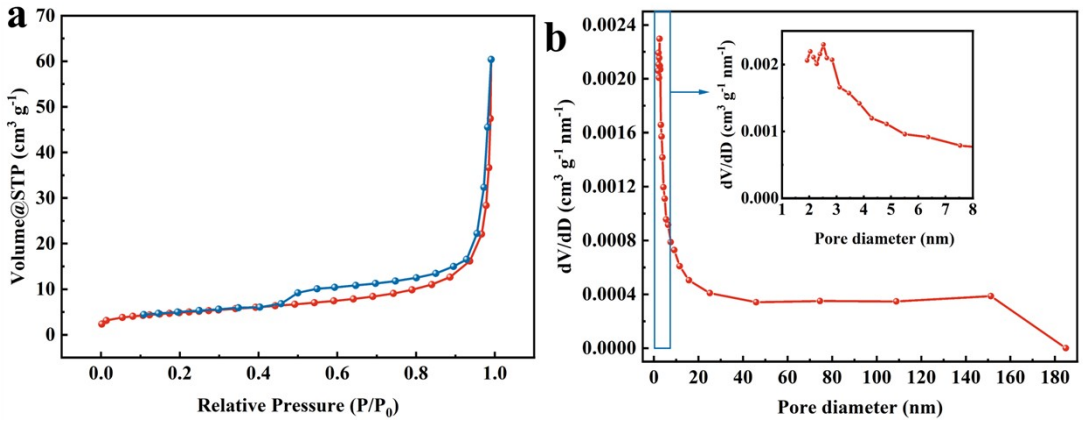

Figure S2. N_2 adsorption-desorption isotherms and corresponding pore size distribution plot of $Sn_2P_2O_7$/rGO.

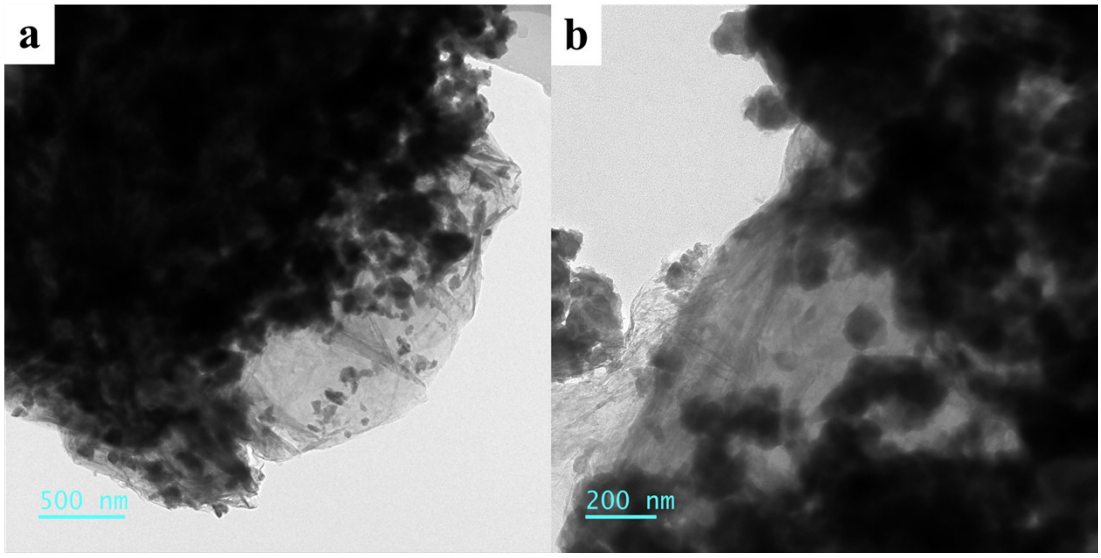

Figure S3. TEM images of $Sn_2P_2O_7$/rGO composite.

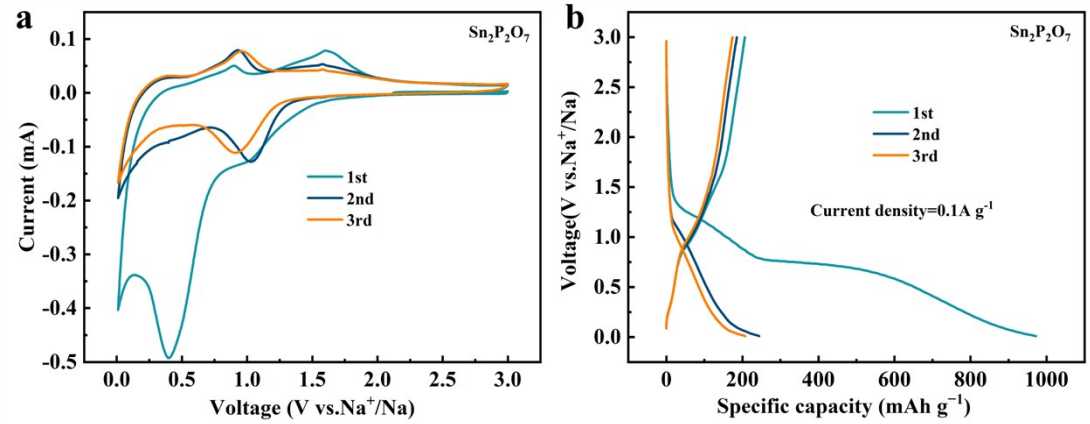

Figure S4. (a) CV curves at a scan rate of 0.1 mV s^{-1} of $Sn_2P_2O_7$ anode. (b) Charge/discharge profiles of the first three cycles at the current density of 0.1 A g^{-1} of $Sn_2P_2O_7$ anode.

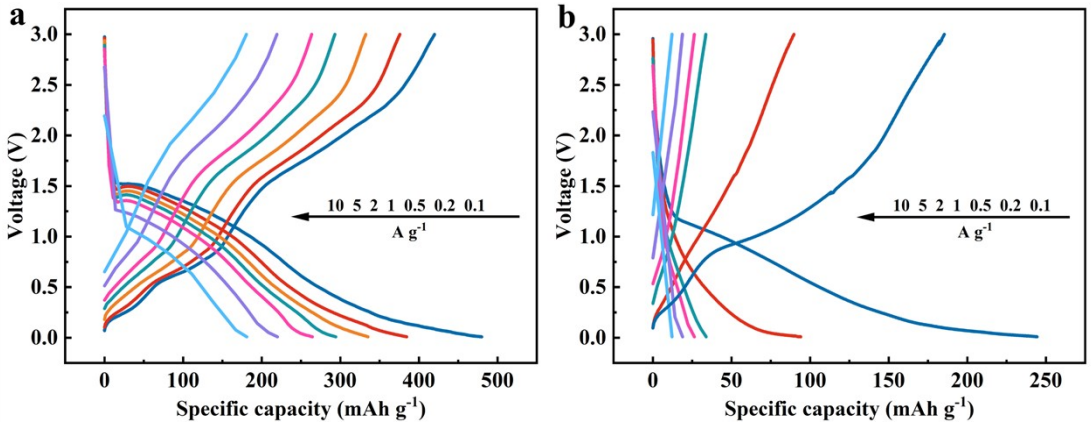

Figure S5. Discharge/charge profiles of (a) $Sn_2P_2O_7$/rGO and (b) $Sn_2P_2O_7$ anodes at different current densities from 0.1 to 10 A g^{-1}.

Table S2. Comparison of rate performance of Sn-based compound/carbon composite anode for SIBs.

Anode materials	Specific capacity/current density (mA h g^{-1}/A g^{-1})	Ref.
$Sn_2P_2O_7$/RGO	(480/0.05) (170/10)	[1]
SnP_2O_7/rGO	(254.7/0.1) (91.1/10)	[2]
SnP_2O_7@N-C	(400/0.1) (210/5)	[3]
SnP_2O_7/NG	(423/0.1) (206/2)	[4]
SnP_2O_7@C	(403/0.2) (110/2)	[5]
SnP_2O_7@C/CN	(342.3/0.1) (106.0/5)	[6]
$Sn_2P_2O_7$/rGO	(433.3/0.1) (185.7/10)	This work

Table S3. Comparison of cycling stability of Sn-based anode materials for SIBs.

Anode materials	Capacity (mA h g^{-1}/A g^{-1})	Cycle life.	Ref.
SnP_2O_7@C/CN	91.5/2	800	[6]
SnS-AB	290/0.1	50	[7]
Sn/Sb@SSO@PCFs	440/0.05	450	[8]
Sn_4P_3@CNF	336/1	500	[9]
Sn_3Se_5@PPy	187.8/5	300	[10]
Sn-Ni@NC	150.3/1	200	[11]
$Sn_2P_2O_7$/rGO	165.4/1	1000	This work

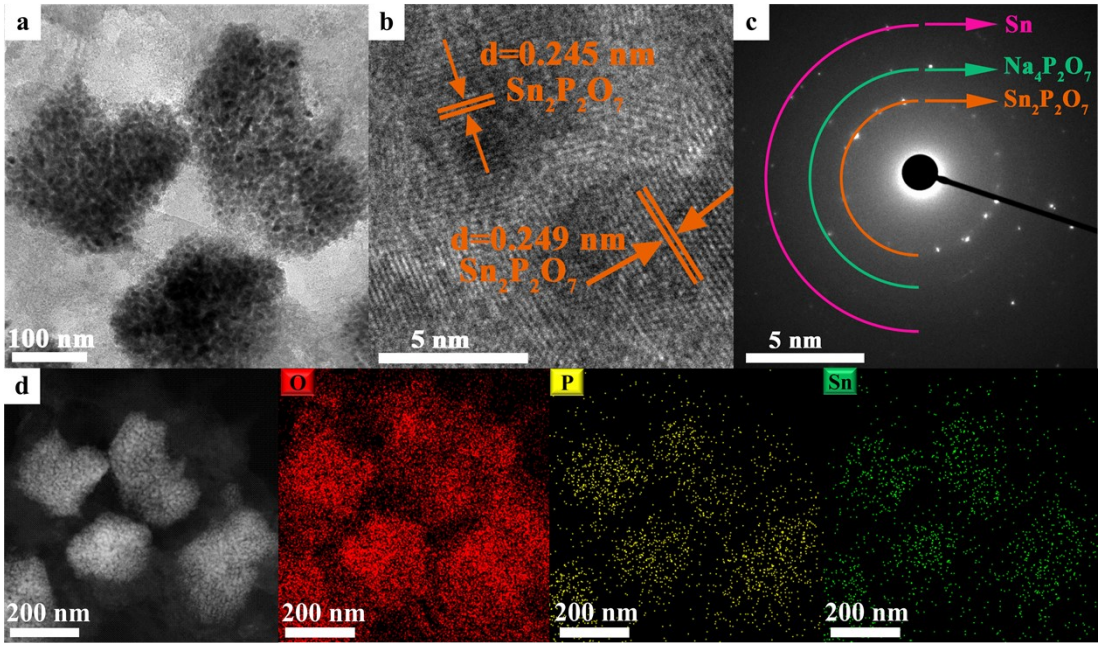

Figure S6. (a) *Ex-situ* TEM images, (b) HRTEM images, (c) SAED patterns and (d) EDS elemental mappings of $Sn_2P_2O_7$ anode after 1000 cycles at a current density of 1 A g^{-1}.

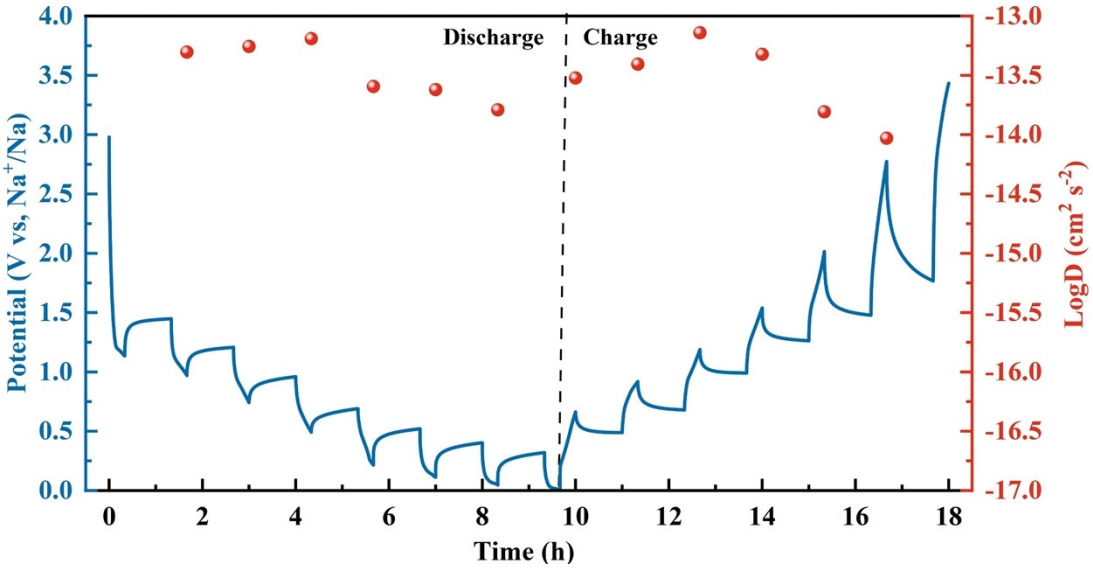

Figure S7. GITT curve and diffusivity versus state of discharge and charge during the selected second cycle of $Sn_2P_2O_7$ anode. (The D_{Na^+} of $Sn_2P_2O_7$ anode ranges from $1\times10^{-13.19}$ cm^2 s^{-1} to $1\times10^{-13.79}$ cm^2 s^{-1} during discharge process, and from $1\times10^{-13.14}$ cm^2 s^{-1} to $1\times10^{-14.03}$ cm^2 s^{-1} during charge process.)

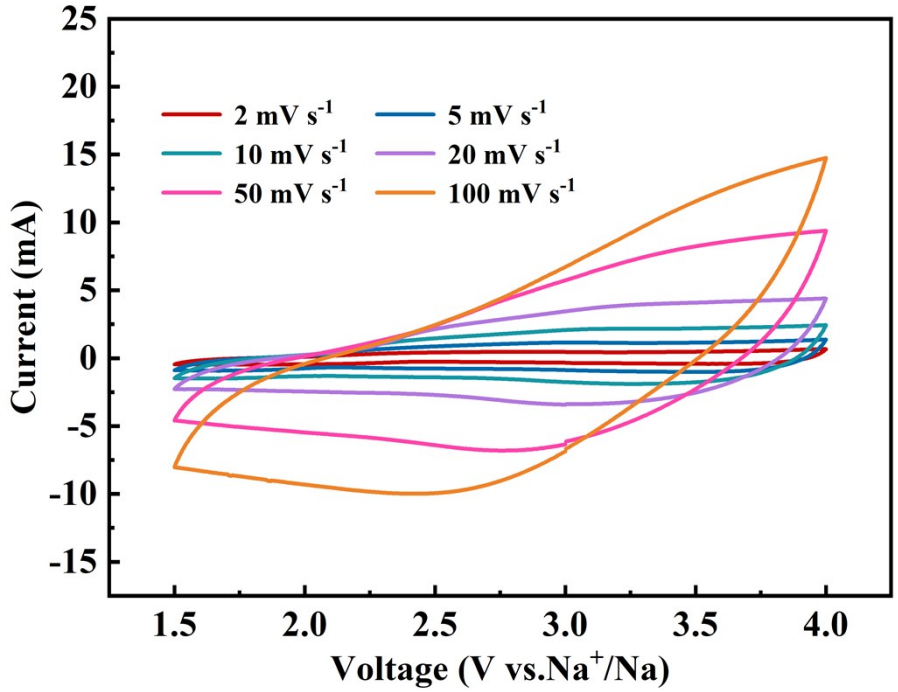

Figure S8. Half-cell performance of the AC vs. Na metal, tested between 1.5−4.0 V. CV curves at different scan rates from 2 mV s^{-1} to 100 mV s^{-1}.

References

1 X. Yang, R. Y. Zhang, J. Zhao, Z. X. Wei, D. X. Wang, X. F. Bie, Y. Gao, J. Wang, F. Du and G. Chen, *Adv. Energy Mater.*, 2017, **8**.

2 J. Pan, S. Chen, D. Zhang, X. Xu, Y. Sun, F. Tian, P. Gao and J. Yang, *Adv. Funct. Mater.*, 2018, **28**.

3 S. Mu, Q. Liu, P. Kidkhunthod, X. Zhou, W. Wang and Y. Tang, *Natl. Sci. Rev.*, 2020.

4 L. Bai, X. Pang, Y. Sun, X. Zhang and J. Guo, *J. Alloys Compd.*, 2021, **854**.

5 W. He, K. Chen, R. Pathak, M. Hummel, B. S. Lamsal, Z. Gu, P. Kharel, J. J. Wu and Y. Zhou, *ACS Appl. Mater. Interfaces*, 2021, **13**, 22577-22585.

6 X. Guo, Z. Wan, D. Wei, X. Zeng, Z. Li, W. Jiang, H. Wang, M. Ling, H. Li and C. Liang, *ChemElectroChem*, 2021, **8**, 2708-2714.

7. W. Wang, L. Shi, D. Lan and Q. Li, *J. Power Sources*, 2018, **377**, 1-6.

8. X. Chen, N. Zhang, P. He and X. Ding, *J. Alloys Compd.*, 2023, **938**, 168472.

9. L. Ran, I. Gentle, T. Lin, B. Luo, N. Mo, M. Rana, M. Li, L. Wang and R. Knibbe, *J. Power Sources*, 2020, **461**, 228116.

10. L.-b. Tang, P. Yang, Y.-j. Chen, P.-y. Li, T. Peng, H.-X. Wei, Z. Wang, Z.-j. He, C. Yan, J. Mao, K. Dai, Y. Cheng, L.-M. Gao and J.-c. Zheng, *J. Power Sources*, 2022, **552**, 232210.

11. H. Li, Y. He, X. Li, J. Yu, X. Sun, T. Gao and G. Zhou, *Applied Surface Science*, 2023, **611**, 155672.